ADVANCED ENERGY MATERIALS
www.advenergymat.de

Photophysics of PbS Quantum Dot Films Capped with Arsenic Sulfide Ligands

Demetra Tsokkou, Paris Papagiorgis, Loredana Protesescu, Maksym V. Kovalenko, Stelios A. Choulis, Constantinos Christofides, Grigorios Itskos, and Andreas Othonos*

PbS quantum dots (QDs) of different sizes capped with short $(NH_4)_3AsS_3$ inorganic ligands are produced via ligand exchange processes from oleate-capped PbS QDs. The solid-state photophysical properties of the control organic-capped and the inorganic-ligand-capped QDs are investigated to determine their potential for optoelectronic applications. Ultrafast transient transmission shows that in the oleate-capped QDs, carrier recombination at sub-nanosecond scales occurs via Auger recombination, traps, and surface states. At longer times, intense signals associated with radiative recombination are obtained. After ligand exchange, the QDs become decorated with $(NH_4)_3AsS_3$ complexes and relaxation is dominated by efficient carrier transfer to the ligand states on timescales as fast as ≈2 ps, which competes with carrier thermalization to the QD band edge states. Recombination channels present in the oleate-capped QDs, such as radiative and Auger recombination, appear quenched in the inorganic-capped QDs. Evidence of efficient carrier trapping at shallow ligand states, which appears more intense under excitation above the $(NH_4)_3AsS_3$ gap, is provided. A detailed band diagram of the various relaxation and recombination processes is proposed that comprehensively describes the photophysics of the QD systems studied.

1. Introduction

Colloidal quantum dots (QDs) combine the attributes of the nanoscale semiconductors with the ease and low-cost solution processing at low temperatures for numerous optoelectronic applications that include light-emitting diodes, lasers, solar cells, and photodetectors.[1–3] Conventionally, colloidal QDs are decorated with long organic hybrocarbon molecules[3,4] to provide surface chemical passivation and colloidal solubility in common organic solvents. However, such ligands act as insulating barriers and inhibit electronic coupling and transport within the arrays of QDs. To overcome these limitations, attention has been recently focused on the replacement of the commonly used long chain ligands with shorter passivating molecules.[5–8] Different strategies have been followed with the solution phase ligand exchange perhaps being the most successful.[9–16]

For PbS QDs, which are of particular interest for infrared (IR) optoelectronic applications,[15,17–20] long chain organic molecules have been successfully exchanged with different smaller organic molecules.[6,10–12] Devices based on such short-ligand PbS QDs exhibited higher photocurrent densities confirming improved carrier transport properties.[10,21] For example, short ligand PbS QD-based solar cells with power conversion efficiencies greater than 5% have been demonstrated.[19,22,23] However, organic linkers are often volatile and prone to oxidation. In the search for more chemically robust surface chemistries, a radically new approach has been demonstrated recently, in which organic ligands are interchanged with chalcogenidometalate or metal free chalcogenides complexes.[5,13–15,24,25] Processing of PbS QDs with chalcogenide complexes renders the QD surface negatively charged and results in a strong electrostatic repulsion between the QDs preventing their aggregation in colloidal solution, while maintaining efficient interdot electronic coupling in thin-film QD solids.[13–15]

Fundamental investigations of these novel inorganic QDs are critical to access and optimize their potential for optoelectronic applications, however very little is known about their photophysics,[13–15] especially in the solid state. Here, PbS QDs of different sizes capped with short $(NH_4)_3AsS_3$ inorganic ligands were produced via ligand exchange reaction from oleate-capped

Dr. D. Tsokkou, Prof. C. Christofides, Prof. A. Othonos
Research Center of Ultrafast Science
Department of Physics
University of Cyprus
Nicosia, 1678, Cyprus
E-mail: tsokkou.demetra@ucy.ac.cy

Dr. D. Tsokkou, P. Papagiorgis, Prof. G. Itskos
Experimental Condensed Matter Physics Laboratory
Department of Physics
University of Cyprus
Nicosia, 1678,Cyprus

L. Protesescu, Prof. M. V. Kovalenko
Institute of Inorganic Chemistry
Department of Chemistry and Applied Biosciences
ETH Zürich, CH-8093, Zürich, Switzerland

L. Protesescu, Prof. M. V. Kovalenko
Empa-Swiss Federal Laboratories for Materials Science and Technology
CH-8060, Dübendorf, Switzerland

Prof. S. A. Choulis
Molecular Electronics and Photonics Research Unit
Department of Mechanical Engineering and Materials Science and Engineering
Cyprus University of Technology, Limassol, 3603, Cyprus

DOI: 10.1002/aenm.201301547

PbS QDs and investigated by a combination of steady-state and time-resolved transmission and photoluminescence (PL) spectroscopies. The experiments cover a wide spectral region from ultraviolet (UV) to near-IR, with temporal resolution from femtoseconds up to microseconds while tuning additional experimental parameters such as excitation wavelength, power, and temperature. Surface recombination in the presence of the inorganic surfactant ligands dominates carrier dynamics, while effects present in the oleate capped QDs, such as radiative and Auger recombination were found significantly suppressed. Carrier trapping at ligand states occurs fast within few picoseconds at states as shallow as ≈10–20 meV below the QD band edge. Based on experimental observations we have developed comprehensive energy diagrams of the various photophysical mechanisms and the respective timescales for the QD systems under study.

2. Experimental Results and Discussion

2.1. Selection of the Capping Ligand: $(NH_4)_3AsS_3$

Previous reports have shown that of all chalcogenidometalate ligands, only arsenic sulfide based species, such as AsS_3^{3-} anions (with Na^+, K^+ or NH_4^+ as counterions) can quantitatively displace oleate ligands on the surface of PbS QDs, while maintaining colloidal stability in polar solvents such as dimethyl sulfoxide (DMSO) and retaining basic optical properties such as bright infrared photoluminescence.[13,15] We concentrate on $(NH_4)_3AsS_3$ rather than K_3AsS_3 or Na_3AsS_3 for the following reasons. While $(NH_4)_3AsS_3$ shows same ability to colloidally stabilize PbS QDs in polar solvents, it easily converts into narrower gap As_2S_3 in a dry state, releasing NH_3 and H_2S. In fact, this decomposition can be aided by heating and is complete below 100 °C. Such low decomposition temperature ensures that the PbS QDs, thermally labile at higher temperatures, remain intact. Besides the recent report on the steady-state and time-resolved infrared photoluminescence of PbS/CdS QDs in As_2S_3 matrix,[15] there have been no systematic photophysical measurements on unpassivated PbS QDs. As discussed in the introduction, the best performing photodetectors and photovoltaic devices are usually obtained with uncoated PbS QDs to ensure efficient carrier separation, thus calling for detailed spectroscopic studies of inorganic-capped PbS QDs as potential candidates for future optoelectronic devices. In support of this expectation for inorganic-capped PbS QDs, Guyot-Sionnest and co-workers have recently reported improved performance of transistors and photodetectors based on HgTe QDs after the ligand displacement with As_2S_3 solutions in propylamine/ethanol.[26]

2.2. Optical Absorption Studies

Steady state absorption spectra of solutions and films of the various sizes PbS QDs capped with oleate and $(NH_4)_3AsS_3$ ligands are shown in the **Figure 1**. For the organic-capped QDs, the characteristic peak of the 1S ($1S_h$ –$1S_e$) transition appears strong, showing negligible spectral shift between solutions and films. The peak in films (solutions) is centered at ≈912 nm (≈912 nm), ≈1117 nm (≈1120 nm), and ≈1502 nm (≈1518 nm) corresponding to QDs with diameters of ≈3 nm, ≈4 nm, and ≈6 nm

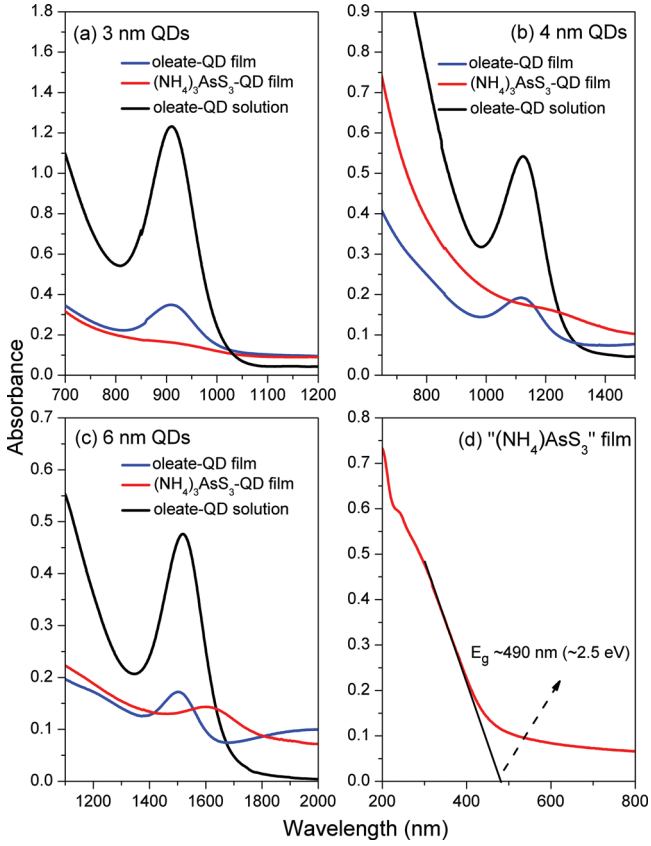

Figure 1. Absorbance spectra of oleate capped PbS QD solutions in chlorobenzene (black) and films (blue), and $(NH_4)_3AsS_3$ capped PbS QDs films (red) of a) ≈3 nm, b) ≈4 nm, and c) ≈6 nm diameter. The absorbance spectrum of the amorphous $(NH_4)_3AsS_3$ ligand film is displayed in the Figure 1d along with its gap estimation.

respectively, as estimated by the empirical equation developed by Moreels et al.[27] In the $(NH_4)_3AsS_3$ capped PbS QDs, an intensity reduction and red shift of the 1S absorbance peak of ≈20, ≈90, ≈60 meV for the ≈3, ≈4, ≈6 nm QDs, respectively is observed. Such effects are usually interpreted as increased overlap of electron and hole wavefunctions of adjacent QDs, enabled by shorter and more conductive inorganic ligands.[24] Wolcott et al. recently studied the dependence of such shifts as a function of interparticle distance on closed packed PbSe QD films and predominantly attributed their origin in the dielectric environment surrounding the QDs.[28] The shifts observed in our data are possibly due to both dielectric and electronic coupling effects. The possibility that the absorption variations are due to modifications in the lattice structure, size, or shape of QDs caused by the ligand exchange process is excluded by the nearly identical X-ray diffraction (XRD) patterns of the QDs before and after ligand exchange (see Figure S1 and relevant discussion in Supporting Information).

Absorption measurements were also carried out on a control film containing the $(NH_4)_3AsS_3$ ligands. The sample appears yellow indicating the release of NH_3 and H_2S from the ligand molecule and the formation of an amorphous film predominantly composed of As_2S_3. The absorption spectrum of the

film is shown in Figure 1d, containing a high energy region up to ≈500 nm and a tale extending to the IR, typical of midgap absorption transitions. From the projection of the high energy side absorbance, an energy band gap of ≈2.5 eV (≈496 nm) is estimated, in proximity to the reported bandgap of ≈2.4 eV for the As_2S_3.[29]

2.3. Time-Resolved Transmission Spectroscopy

Differential pump–probe transmission spectra from the organic and inorganic-capped ≈3 nm PbS QDs are displayed in **Figure 2**a,b. Pumping at 400 nm with moderate pump fluences of 0.5 mJ cm^{-2} and several visible (Vis) and near-IR probing pulses were employed. The same pump fluence was used for both samples to photogenerate approximately equal carrier densities, as the two films exhibit similar absorbance at the selected excitation wavelength of 400 nm.

In agreement with previous findings for the ≈3 nm oleate-capped PbS QDs,[30] free carrier absorption effects dominate all the Vis probing wavelengths as indicated by the negative differential transmission of Figure 2a. In the probing spectral region of 550–650 nm, a long rise time between ≈1–1.5 ps is recorded (inset of Figure 2a), characteristic of the relatively long carrier relaxation time to the probed energy levels. State filling effects

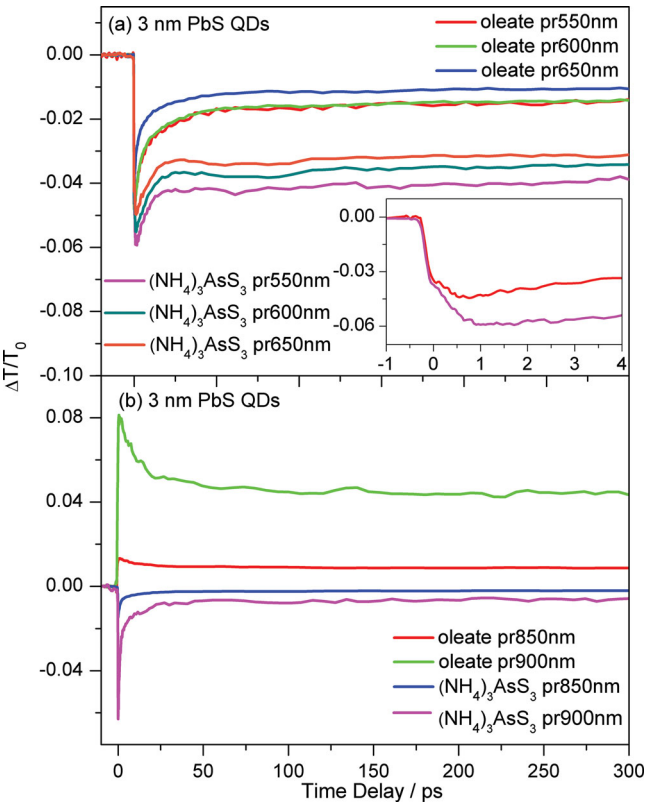

Figure 2. Non-degenerate transmission change measurements of 3 nm oleate and $(NH_4)_3AsS_3$ capped PbS QDs using pump pulses at 400 nm, pump fluence of 0.5 mJ cm^{-2} and probe pulses at a) 550–650 nm and b) 850–900 nm, respectively. In the inset of (a), the first 4 ps are shown when probing at 550 nm.

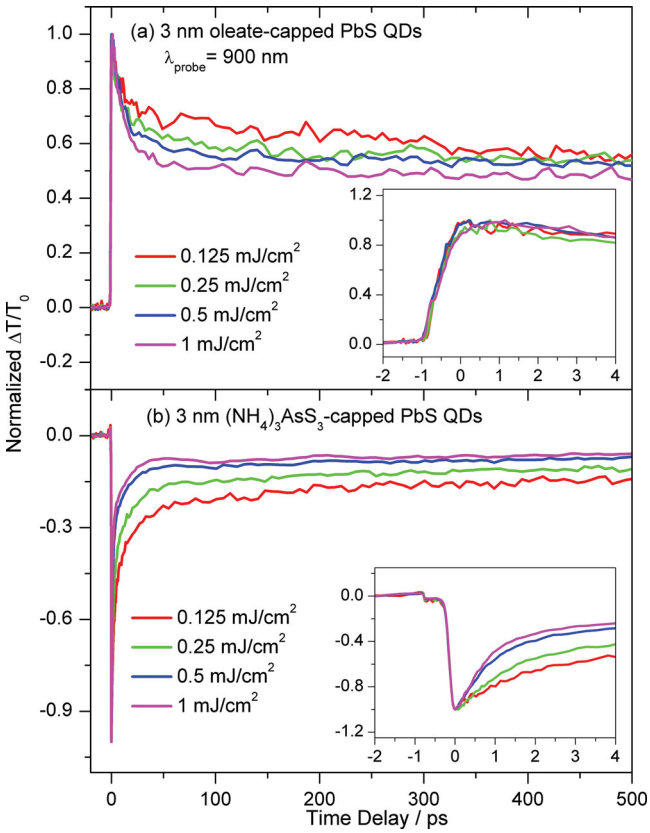

Figure 3. Intensity-dependent transmission change measurements of 3 nm a) oleate and b) $(NH_4)_3AsS_3$ capped PbS QDs using pump pulses at 400 nm, probing at 900 nm, and pump fluences between 0.05 and 1 mJ cm^{-2}. The first 4 ps are shown in the insets.

(positive signal) are evident for the wavelength region of 850–900 nm (Figure 2b) that coincides with the QD 1S transition. Probes across this region monitor the QD ground states that become partial filled following relaxation of the photoexcited carriers.

The transient decays of the arsenic sulfide-capped PbS QDs exhibit different characteristics. For Vis (IR) probes the decays appear slower (faster) than the respective decays in the organic-capped QDs. Furthermore, no QD state filling effects are observed for all probes for times up to 500 ps. To further investigate the different transient behavior of the two QD systems, intensity dependent measurements at 900 nm were carried out. Normalized data are shown in **Figure 3**a,b.

The intensity measurements verify the small carrier occupancy of the ground state of the $(NH_4)_3AsS_3$-capped QDs for pump fluences up to 1 mJ cm^{-2} suggesting the presence of efficient relaxation channel(s) that deplete these states. Such fast relaxation channel(s) do not appear in the oleate capped dots so they should originate at the different surface environment of the QDs. The possibility that the small filling of the inorganic-capped QD core states results from direct photoexcitation of carriers at the ligand states has to be ruled out as $(NH_4)_3AsS_3$ absorption (see Figure 1d) is orders of magnitude smaller than the respective absorption by the QD states at 400 nm. The pump pulse then predominantly photogenerates hot carriers in

the QD state continuum in both types of QDs. In the oleate-capped QDs, carriers relax at picosecond scale and fill the QD quantized states. In the $(NH_4)_3AsS_3$ capped QDs instead, such states are efficiently depleted and the transient signal is dominated by photoinduced absorption to higher states. The signal in this case exhibits a pulse width limited rise time (inset of Figure 3b) faster than the approximately picosecond cooling time to the QD band edge states (see inset of Figure 3a), which indicates that high energy QD states are probed and that a large fraction of the carriers are captured by the inorganic ligand/surface states before being thermalized.

Figure 3 demonstrates that in both QD systems the relaxation dynamics depend on the pump fluence. The recovery at early times becomes faster for higher fluences indicating the presence of Auger recombination.[30,31] The effect can originate either from multiple excitons generated by the absorption of equal number of photons per QD or via multiexciton generation from a single photon per QD.[32,33] In our case, the first mechanism dominates as the energy threshold for multiexciton generation for ≈3 nm PbS QDs was shown to be around 2.35 times the energy QD gap[33] (i.e., a wavelength of ≈380 nm), which is higher than the pump photon energy used. Following the previous discussion, in the organic-capped QDs Auger occurs subsequent to carrier cooling in the QD core states. On the other hand, in the inorganic-capped QDs the efficient depletion of the QD ground states (i.e., absence of state filling effects) may allow Auger recombination from higher lying QD states to be observed. This is consistent with the higher Auger rates observed in the arsenic sulfide-capped QDs at early timescales (inset of Figure 3b) compared to those of oleate capped QDs (inset of Figure 3a).

Fits to the experimental data at the lowest pump fluence using multiexponential functions reveal the temporal differences in the relaxation pathways in the two QD systems. Under the low fluence of 0.125 mJ cm^{-2}, Auger effects are expected to have a negligible influence on the QD carrier dynamics. For the oleate capped QDs a biexponential decay function of the following form is required to describe the experimental data from the oleate capped PbS QDs,

$$\Delta T/T_0 = A_0 + A_1 e^{-t/t_1} + A_2 e^{-t/t_2} \quad (1)$$

where $A_{1,2}$ are the relative amplitudes of the relaxation channel with time constants of $t_{1,2}$ respectively. A fast decay of 10 ps with a relative amplitude of 25% is assigned to carrier relaxation to shallow donor surface states, as previously confirmed for oleate-capped PbS QDs.[34,35] A second channel of hundreds of picoseconds (≈590 ps) with a relative amplitude of 30% is typically associated with non-radiative recombination to traps. The constant coefficient A_0 with a high relative amplitude of ≈45% has to be included to achieve a satisfactory fitting, given that a large proportion of carriers in these QDs recombine at much longer times than the timescale of the pump-probe experiments. Recombination at such timescales is dominated by radiative recombination as evidenced by the analysis of the time-resolved PL experiments presented later in the text.

Fitting of the transient decays of the $(NH_4)_3AsS_3$-capped PbS QDs requires a triexponential decay function. It appears that half of the photogenerated carriers relax with a very fast time constant of ≈2 ps. Based on the previous discussion, the relaxation mechanism is attributed to fast trapping of hot carriers into surface/ligand states. From the rest of the carriers, 30% relax within a 20 ps decay, probably associated with the relaxation of hot carriers to deep ligand states. The significantly longer channel in the range of nanoseconds is most likely associated with recombination of carriers within the QD core states.

To explore the effect of QD size on the carrier dynamics, intensity measurements have been carried out for PbS QDs of ≈3, ≈4, and ≈6 nm, capped with both kinds of ligands and probe pulses at 600 nm. The experimental data are presented in **Figure 4**. In all cases, a positive differential transmission signal due to free carrier absorption effects is dominant, while no significant variations in the magnitude of the differential transmission for the different samples were observed. The slow rise time in the picosecond range detected in all data, indicates that the carriers probed at both QD systems have been thermalized following their 400 nm pump photoexcitation. This is in contrast with the pulse width limited rise time recorded at the decays of the arsenic sulfide-capped QDs when probing at 900 nm (see Figure 3b). Visible (600 nm) and infrared (900 nm) probing at the inorganic-capped QDs, results then in investigations of the dynamics of thermalized and hot carriers, respectively.

In the oleate-capped PbS QDs, transient decays appear strongly dependent on the excitation fluence for all QD sizes. The increase of the relaxation rate with laser intensity is strongly suggestive of efficient Auger recombination (Figure 4a–c). For the same pump fluence of 0.5 mJ cm^{-2}, Auger rates tend to increase with QD size (inset of the Figure 4c); similar trends are also observed for the rest of the pump fluences. A possible explanation relies on the presence of multiexciton effects.[32,36] As the same pump photon energy is used to excite all QDs, multiexciton generation is more effective for lower gap dots, i.e., bigger QDs, resulting in higher multiexciton generation yield. Commonly such effects are manifested in the optical data by the Auger recombination of the produced multiexcitons, which can explain the increase in the Auger rate with QD size.

A different temporal behavior is observed in the decays of the inorganic capped PbS QDs presented in Figure 4d–f. For the ≈3 nm QDs, contribution from Auger recombination is still evident, however it results in weaker dependence on the pump fluence compared to that exhibited by the ≈3 nm sized oleate capped QDs. The behavior is more pronounced for larger QDs where contribution from Auger becomes negligible and carrier dynamics become independent of the pump fluence. The quenching of Auger recombination is attributed to the unfavorable competition with the efficient trapping to the ligand/surface states. The temporal profile of the decays follow a double exponential decay with a fast time constant of few picoseconds (≈8–13 ps) and a significantly slower one in the range of nanoseconds (≈1.4–1.9 ns). Following the same reasoning with that previously used for the IR probing decays that show channels with similar timescales (**Table 1**), the fast decay is attributed to ligand trapping and the longer channel to trap recombination. In this case the decays have been associated with carriers thermalized to the bottom of the QD band edges so relaxation occurs from the QD band edge to shallow

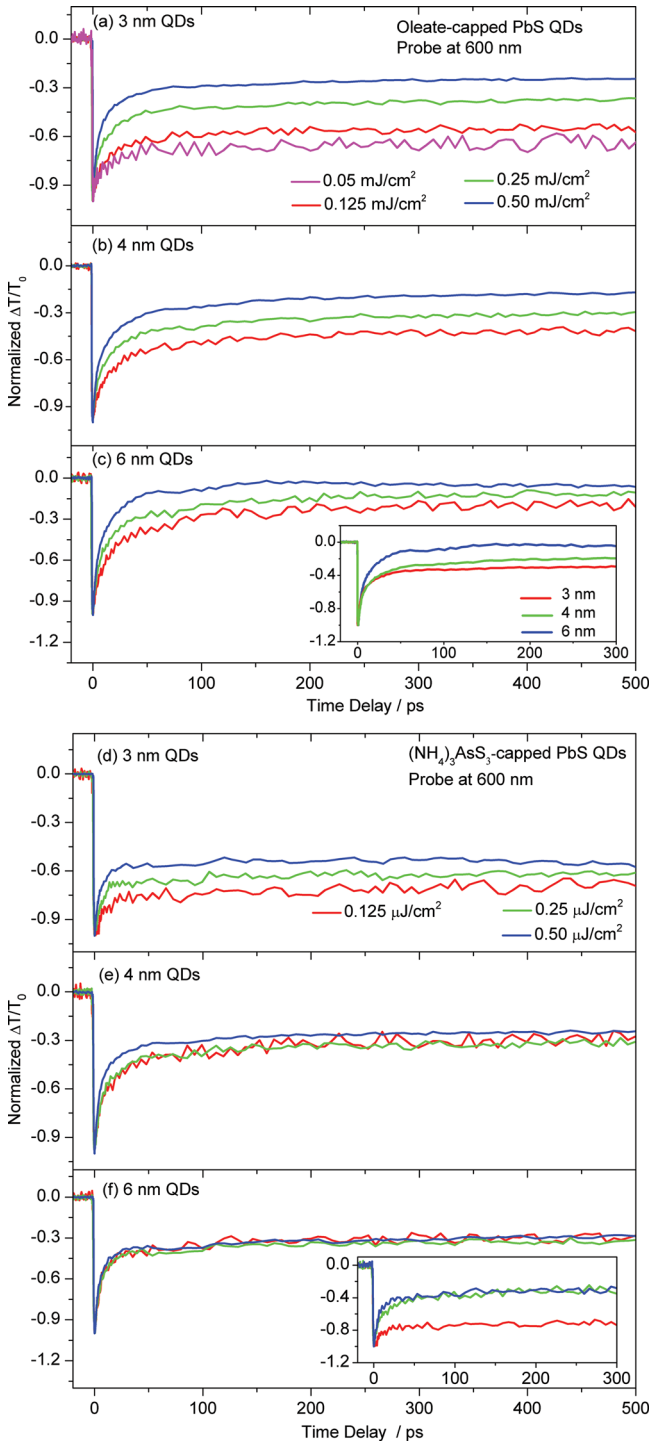

Figure 4. a–c) Intensity-dependent normalized differential transmission of oleate-capped PbS QDs and d–f) $(NH_4)_3AsS_3$ capped PbS QDs of 3 nm, 4 nm, and 6 nm, using pump pulses at 400 nm, probing at 600 nm with pump fluences between 0.05 and 0.50 mJ cm^{-2}. In the inset of the Figure 4c, the normalized differential transmission of organic capped PbS QDs of different size at pump fluence of 0.50 mJ cm^{-2} is shown. In the inset of Figure 4f, the data for $(NH_4)_3AsS_3$ capped PbS QDs of different size using a pump fluence of 0.125 mJ cm^{-2} are shown.

Table 1. Fitting parameters of relaxation times and relative amplitudes, based on multiexponential decays for 3 nm oleate and $(NH_4)_3AsS_3$ capped PbS QDs probing at 900 nm and pump fluence of 0.125 mJ cm^{-2}.

Sample	A_0	A_1	t_1 [ps]	A_2	t_2 [ps]	A_3	t_3 [ns]
Oleate capped QDs	0.45	0.25	10	0.3	590	—	—
$(NH_4)_3AsS_3$ capped QDs	—	0.5	2	0.3	20	0.2	1.1

ligand states, as evident in the PL measurements presented later within the text.

2.4. Photoluminescence Spectroscopy

To further investigate the recombination mechanisms and enable distinction between radiative and non-radiative channels, systematic studies of steady-state and time-resolved PL experiments were performed. The normalized steady state PL spectra of ≈3 nm and ≈4 nm PbS QDs for both ligand species taken at 77 K are presented in **Figure 5**a. The spectra were obtained using an ultraviolet (UV) excitation source at 375 nm, in close proximity to the excitation wavelength used in pump–probe experiments. Room temperature (300 K) PL measurements showed similar trends however the signal to noise ratio, especially from the $(NH_4)_3AsS_3$-capped QDs, was significantly deteriorated. The PL spectrum of the ≈6 nm QDs could not be reliably measured due to the weak response of our detector for wavelengths above 1700 nm. As observed in the absorption spectra, a combination of enhanced electronic coupling and dielectric effects redshifts the PL peaks of the inorganic capped QDs by 90–100 meV compared to the same QDs before ligand exchange. At the same time the PL integrated area is reduced by 1–3 orders of magnitude compared to that of the organic-capped QDs, suggestive of enhanced non-radiative recombination mediated by the inorganic ligand states. The results are in agreement with the pump–probe data findings and consistent with the general consensus that a decrease of the QD capping ligand length results in an increased carrier capture rate by the ligands.[37]

PL measurements were also performed under near-IR (785 nm) excitation (see Supporting Information Figure S2). Based on recent precise measurements of PbS QD electronic states,[38] the laser photoexcites the carriers for both ≈3 and ≈4 nm QDs below the $1P_h$-$1P_e$ transition, populating directly the $1S_{e,h}$ QD levels; in the case of the larger dots, the weaker asymmetric 1S-1P transitions may also be excited by the 785 nm laser.[38] For the oleate capped dots, such an excitation results in substantially weaker emission, following the respective drop in the film absorbance. The arsenic sulfide-capped QDs exhibit however an anomalous behavior, with photoexcitation at the 1S QD states (785 nm) resulting typically in higher PL signal than that obtained under excitation at the QD high energy continuum (375 nm). As a result, a significantly smaller emission quenching is obtained in the former case in respect to the emission of the organic-capped dots. The results suggest that in the inorganic capped PbS QDs, photogenerated carriers with excess kinetic energy follow different relaxation

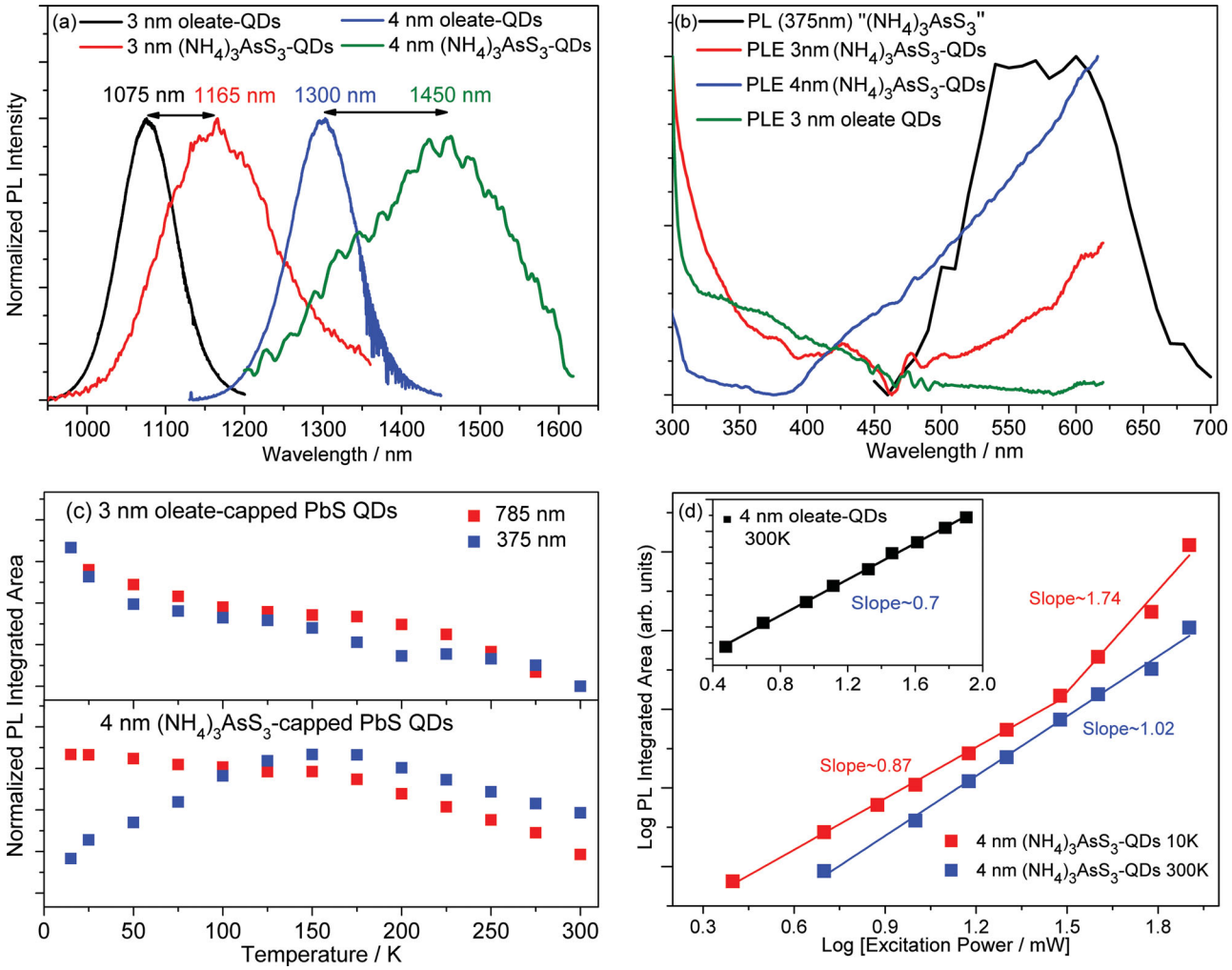

Figure 5. a) Normalized PL spectra of 3 nm and 4 nm QDs films capped with oleate and $(NH_4)_3AsS_3$ ligands excited at 375 nm. b) Normalized PL spectrum of the $(NH_4)_3AsS_3$ film at 375 nm and PLE spectra of the $(NH_4)_3AsS_3$ capped, 3 and 4 nm QDs. All measurements were performed at 77 K. c) Temperature dependence of the integrated PL area of 3 nm oleate-capped PbS QDs (top) and 4 nm $(NH_4)_3AsS_3$ capped PbS QDs (bottom) following excitation at 375 nm and 785 nm. The data were normalized to the peak integrated area. d) Log–log plots of the PL integrated area for the 4 nm $(NH_4)_3AsS_3$ capped PbS QD film as a function of excitation power following excitation at 785 nm. The respective best square fits are shown with solid lines. The respective results for the 4 nm oleate capped QDs at room temperature are displayed in the inset of (d).

paths to those thermalized in the ground states, contributing differently to the PL emission. Hot carriers generated by UV excitation are captured fast by the ligand states. On the other hand, surface trapping of carriers photogenerated within the QD 1S states is less efficient, resulting in higher yield of radiative recombination.

PL measurements were also performed in the control $(NH_4)_3AsS_3$ ligand film. The associated spectrum, presented in Figure 5b, was recorded at 77 K following photoexcitation at 375 nm. The film exhibits a very weak, broad PL band centered at ≈580 nm, which is order(s) of magnitude weaker than the PL from the QDs. No PL signal was detected from the ligand film under IR (785 nm) excitation. Taking into account the estimated from the absorption data, energy gap of the ligands (≈2.5 eV), the PL signal could be due to arsenic sulfide band-to-band emission. To further investigate the role of the ligand states in the radiative recombination process, excitation PL (PLE) measurements monitoring the QD PL peak were performed in the spectral region of 300–625 nm. Characteristic spectra obtained at 77 K are shown in Figure 5b. PLE from the ≈3 nm organic capped QD film drops qualitatively similar to absorption in the 300–625 nm range. On the other hand, the PLE spectra from the $(NH_4)_3AsS_3$ capped QDs indicate an increase in the QD emission for excitation wavelengths longer than 400–450 nm. The behavior suggests a higher capture yield of carriers at the QD relative to ligand states, as the excitation energy drops closer and below the ligand band gap (≈490 nm). The model is consistent with the pump–probe data and interprets the anomalous behavior of the inorganic-capped QD PL signal under UV and IR excitation. Such behavior is not observed in the case of oleate capped QDs due to the insulating nature of such ligands.[39]

To further investigate the recombination mechanisms, temperature-dependent PL measurements were performed for PbS QDs with both types of ligands using excitation at the QD continuum (375 nm) and QD 1S states (785 nm). Typical plots of the normalized PL integrated area as a function of temperature are displayed in the Figure 5c. The raw PL spectra versus temperature are included in Figure S3 (Supporting Information). The PL temperature dependence of the ≈3 nm and ≈4 nm oleate capped PbS QDs is fairly typical for such a material.[12,34] As temperature increases, electron–phonon scattering and trap/surface recombination become more efficient at the expense of radiative recombination and the PL signal quenches. A plateau between 125 and 175 K is suggestive of weak carrier redistribution processes within the QDs.[35] Interestingly, the temperature dependence of the PL integrated signals obtained under near-IR (red squares) and UV (blue squares) excitation, follow similar trends. The PL peak also exhibits the expected blue shift with temperature (see Supporting Information, Figure S3a) due to the anomalous PbS lattice temperature coefficient.[40–42]

On the contrary, the PL temperature dependence of the arsenic sulfide-capped QDs (Figure 5c and Supporting Information Figure S3) shows an anomalous behavior, especially following UV photoexcitation at high energy QD states. The PL integrated area increases initially with temperature and subsequently decreases at high temperatures following the behavior shown by the organic capped PbS QDs. Furthermore, the PL peak wavelength remains constant or slightly red shifts with temperature (see Supporting Information Figure S3b). The anomalous behavior of the peak wavelength and intensity with temperature is characteristic of thermally activated detrapping carrier processes. The increase of the temperature provides trapped carriers with enough thermal energy to escape and be recaptured by the QD core states. The behavior is observed up to temperatures of ≈125–200 K, thus suggesting that trapping occurs at shallow ligand states in the range of 10–20 meV.

Further information about the QD recombination processes was obtained via excitation dependent PL experiments performed on the two QD systems using an excitation at 785 nm, quasi-resonant to the QD ground states. The log–log summary plots at 10 K and 300 K and the respective least-square fits for the ≈4 nm $(NH_4)_3AsS_3$ capped PbS QDs are shown in Figure 5d. In the inset of this Figure, results for the 4 nm oleate PbS QDs at 300 K are also depicted for comparison. The excitation power dependent behavior of the organic capped QDs closely resembles the trends of our previous reported studies on PbS QDs.[43] The fits reveal a sublinear dependence with slope of ≈0.7 that suggests Auger as the dominant recombination mechanism; the expected slope in this case is ≈0.67.[44] A similar slope of ≈0.72 has been obtained from the ≈3 nm oleate-capped QD film at 300 K. The behavior of ≈4 nm and ≈3 nm (Figure S4, Supporting Information) $(NH_4)_3AsS_3$ capped QDs appears more complex. At low temperature (10 K), the slope of the log-log plot changes from sublinear (≈0.43 for the ≈3 nm QDs, ≈0.87 for the ≈4nm QDs) to linear (≈3 nm QDs) or superlinear (≈4 nm QDs) as the excitation power is increased. The slope change indicates a trap (ligand) limited recombination of carriers. Based on the previous discussion, the low excitation regime is dominated by the ligand recombination responsible for the observed sublinear behavior. As the excitation power increases, ligand states become saturated and surface recombination can be surpassed by competing monomolecular or bimolecular processes. At room temperature (300 K), a linear slope is obtained from both of the arsenic sulfide capped QDs indicating monomolecular recombination. The channel should be predominantly non-radiative in nature, as the PL signal appears very weak at 300 K. It is interesting that the studies show no evidence of Auger recombination, in general agreement with the suppressed Auger obtained from the pump–probe experiments described previously.

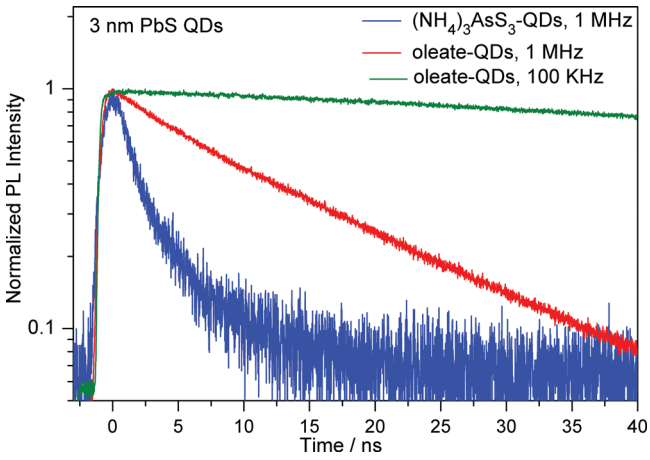

Figure 6. Room temperature PL decays of the 3 nm PbS QDs films capped with oleate and $(NH_4)_3AsS_3$ ligands, excited at 375 nm excitation and recorded at the maximum emission wavelength within a 30 nm spectral window.

Figure 6 shows the room temperature time resolved PL decays of the ≈3 nm PbS QDs capped with oleic acid and $(NH_4)_3AsS_3$ ligands. The decays were obtained while monitoring the QD emission peak using the line of a 375 nm picosecond laser operated at a relatively high repetition rate of 1 MHz. The results at a low repetition rate (100 KHz) in the case of oleate capped QDs are also shown. Measurements were also performed for the 4 nm PbS QDs with quantitatively similar results (not shown). Under high repetition rate, the ≈3 nm organic-capped QD film exhibits a monoexponential decay with a lifetime of ≈15 ns. A decrease in the repetition rate by a factor of 10 (100 KHz) results in a concomitant lifetime enhancement by a factor of ≈9.3 (≈140 ns) for the ≈3 nm oleate-capped PbS QDs. The significant faster decays at higher repetition rates are typically attributed to the presence of additional high frequency-activated QD recombination channels that include multiexciton and photocharging effects.[45] It is noted that no further reduction of the PL lifetime is observed when the laser repetition rate is reduced below 100 KHz. Based on this, the ≈140 ns can be considered as a rough estimate of the radiative lifetime of the ≈3 nm oleate capped QD film.

In the case of the arsenic sulfide capped PbS QDs increase of the laser repetition rate results instead in a weak increase of the TR-PL lifetime, up to a factor of ≈1.5 (see Supporting Information Figure S5). It is possible that carrier depletion of ligand states at high laser frequencies is incomplete, resulting in suppression of the surface recombination and thus of the

overall recombination rate. In any case the behavior is not consistent with the Auger or photocharging effects observed for the organic-capped QDs. The decays of the inorganic-capped QDs show biexponential kinetics with a dominant fast decay of the order of ≈1 ns and a weaker longer decay, varying in the 5–10 ns range (Figure 6). The longer decay is most probably the radiative QD lifetime, quenched compared to the respective radiative lifetimes of the organic-capped dots by a factor ranging from ≈10 to ≈30. A potential origin of the quenching is the higher dielectric constant of the inorganic surface environment. This has been convincingly shown for studied solutions of such organic and inorganic QD materials by Kovalenko et al.[15] Following the relevant derivation and using dielectric constants of ≈17, ≈2.5, and 5.1 for PbS, oleic acid and $(NH_4)_3AsS_3$ materials respectively, a dielectric-induced quenching of the radiative lifetime by a factor of ≈3.9 is calculated. This is significant smaller than the experimental quenching factors observed, i.e., 10–30 as stated above, which indicates that in addition to dielectric screening, other factors contribute to the lifetime shortening. Additional interactions in the solid state, such as enhanced interdot interactions enabled by the short arsenic sulfide ligands, can influence the electron-hole wavefunction overlap and result in the further shortening of the radiative lifetime.

2.5. Energy Band Diagrams for the Oleate and Arsenic Sulfide Capped PbS QDs

Based on the information provided from the experimental studies presented, band diagrams with the relaxation/recombination processes and the associated timescales for the oleate and $(NH_4)_3AsS_3$ capped PbS QDs are drawn in **Figure 7**a,b, respectively. For simplicity the diagrams refer to ≈3 nm QDs; similar diagrams can be obtained for the ≈4 nm QDs. The approximate highest occupied molecular orbital (HOMO)/lowest unoccupied molecular orbital (LUMO) QD energy levels values were obtained from ref. [35] and experimentally measured by cyclic voltammetry for PbS QDs of identical sizes.

In oleate-capped PbS QDs, UV (375 nm)/blue (400 nm) excitation denoted with a blue arrow in Figure 7a, results in the generation of carriers at the QD state continuum. The carriers thermalize to the conduction/valence band edges (Process A) within 1–1.5 ps. A fraction of the electrons is captured by shallow donor states with a time constant of 10 ps (Process B). The rest of the carriers recombine nonradiatively/radiatively within hundreds of picoseconds (≈600 ps, Process C) or hundreds of nanoseconds (≈140 ns lifetime, Process D), respectively. In addition to these mechanisms, additional sub-nanosecond channels (not drawn) become activated at elevated excitation densities that include Auger recombination and multiexciton effects.

In the $(NH_4)_3AsS_3$-capped PbS QDs, a more elaborate diagram is drawn to demonstrate the new photophysical processes observed, which include recombination mediated by the metal chalcogenide ligands (Figure 7b). Electron affinity of $(NH_4)_3AsS_3$ is assumed similar to As_2S_3 ≈3.6 eV[46]; the ligand gap is obtained from the absorption/PLE measurements to

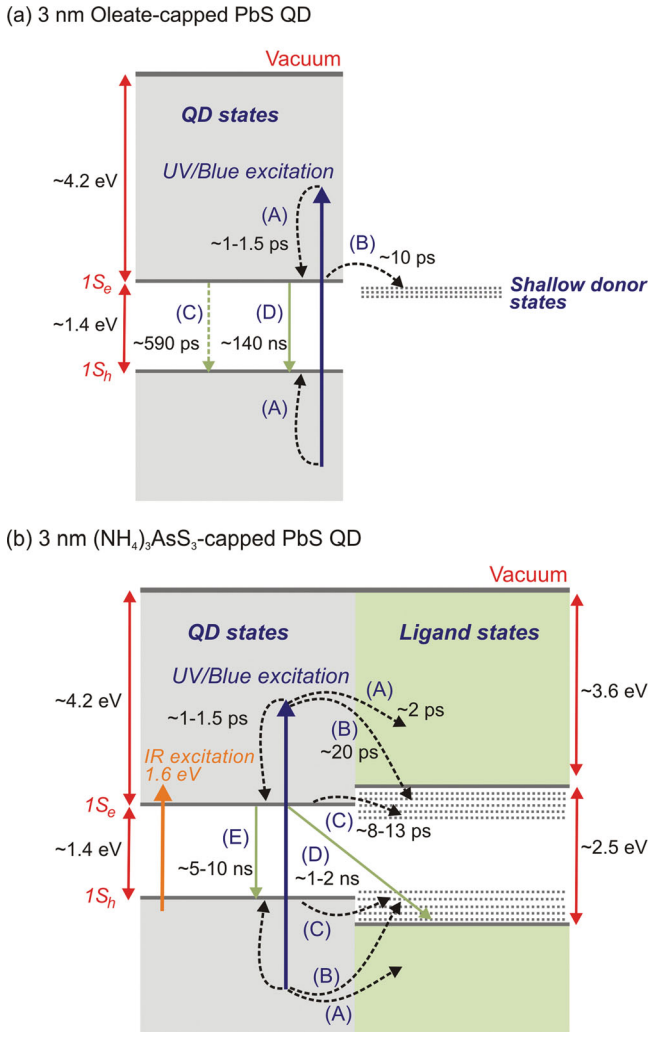

Figure 7. Schematic energy band diagrams of a) 3 nm oleate-capped PbS QDs and b) 3 nm $(NH_4)_3AsS_3$ capped PbS QDs with various relaxation mechanisms following carrier photoexcitation with UV/blue radiation (blue arrow) and IR radiation (orange arrow).

be ≈2.5 eV. The derived diagram suggests that PbS QDs and $(NH_4)_3AsS_3$ ligands form a type I energetic band alignment. Following UV (375 nm)/blue (400 nm) excitation, a large fraction of the carriers is captured at timescales of ≈2 ps before being thermalized (Process A). A longer relaxation time in the range of tens of picoseconds (≈20 ps) is related to the combined processes of carrier capturing and relaxation within the ligand states (Process B). Following near-IR excitation, carriers populate directly the QD 1S states. A fraction of them, transfers to the ligand states within few ps (≈8–13 ps, process C). There is evidence from the temperature dependent PL that significant trapping occurs at shallow states located within 10–20 meV below (above) the LUMO (HOMO) QD levels. For the carriers that escape trapping, recombination occurs via two channels at timescales of ≈1–2 ns and ≈5–10 ns attributed to QD nonradiative (Process D) and radiative recombination (process E), respectively.

3. Conclusions

A combination of steady-state and time-resolved absorption and luminescence techniques has been used to provide insight into the photophysics of films of PbS QDs capped with short arsenic sulfide ligands, produced via ligand exchange processes from oleate capped dots. Such newly discovered inorganic-capped QDs appear promising as stable and functional building blocks for electronic devices, however their solid-state properties have remained unexplored. In our investigations, a plethora of experimental parameters such as QD size, excitation wavelength, power, and temperature have been varied and the main QD relaxation and recombination processes have been identified and analyzed. Based on the experimental findings, a comprehensive energy diagram describing the photophysics of the $(NH_4)_3AsS_3$ capped PbS QD films has been drawn. Overall, our study indicates that the ligand exchange process introduces arsenic sulfide states above and below the QD band edge levels that act as efficient sinks of carriers, resulting in strong modifications in the carrier recombination mechanisms and times. The observed suppression of Auger recombination and photocharging effects in the $(NH_4)_3AsS_3$ capped PbS QDs may be promising as both mechanisms are limiting factors in the operation of QD-based optoelectronics. Such attributes, along with the potential of passivation with a plethora of other unexplored and potentially better chalcogenidometalates, make such all-inorganic quantum dots a highly promising quantum dot material system.

4. Experimental Section

Oleate PbS QDs were synthesized following a process similar to that reported by Hines et al.[47] The PbS nanoparticles capped with oleate ligands were dissolved in chlorobenzene. Next, a solution phase ligand exchange was performed, where the oleate ligands were replaced with the metal chalcogenide complex $(NH_4)_3AsS_3$ and DMSO was used as a solvent. More information is extensively given in ref. [15]. For spectroscopic purposes, all examined oleate capped QDs and inorganic capped QDs of different size between 3–6 nm were deposited on thin quartz substrates. Doctor blading, drop casting, and spin coating have been attempted as deposition techniques for the films; best quality films were obtained using the latter method at 80 °C.

Steady-state absorption of QD solutions and films was performed via a UV/VIS/IR spectrophotometer. Steady state PL spectra were excited by a 375 nm or a 785 nm laser, mechanically chopped at frequencies of 10–20 Hz while operating in the 1–100 mW power range. The luminescence was collected and analyzed using a 0.75 m spectrometer equipped with a charge-coupled device (CCD) camera for the visible region and an InGaAs array detector for the infrared up to 1700 nm. Time-resolved PL spectroscopy was performed using a spectrometer-based time-correlated single photon counting method. Two picosecond laser diodes at 375 and 785 nm with a variable repetition rate in the range of 50 KHz to 1 MHz were employed to excite the PL signal. All PL measurements were carried out under vacuum conditions (10^{-3} mbar), while for temperature-dependent measurements the samples were loaded either into a liquid nitrogen cryostat (77–300 K) or a closed cycle (10–300 K) optical refrigerator.

Time-resolved transmission spectroscopy experiments were carried out using mode-locked ultrashort pulses from an ultrafast amplified Ti:sapphire laser system composed by an oscillator (Tsunami, Spectra Physics) and a regenerative amplifier (Spitfire, Spectra Physics). The output pulses at a repetition rate of 1 kHz have a time duration of 120 fs, central wavelength at 800 nm, and energy of 1.1 mJ per pulse. Non-degenerate pump-probe experiments were performed in a non-collinear geometry. Femtosecond visible wavelength pulses at 400 nm were generated in a second harmonic β-barium borate (BBO) crystal and used to photoexcite the sample, while white light continuum pulses covering a spectral range within 500–1000 nm detected the changes induced to the sample. By varying the temporal delay between the pump and probe pulses, time-resolved photoinduced transmission change was scanned for times up to 500 ps. In non-degenerate transient measurements, PbS QDs on quartz substrates were photoexcited using pump pulses with time duration of 150 fs and pump fluence of 0.5 mJ cm^{-2}. All measurements were performed at room temperature under inert nitrogen atmosphere to avoid sample photodegradation.

Supporting Information

Supporting Information is available from the Wiley Online Library or from the author.

Acknowledgements

The work was co-funded by the European Regional Development Fund and the Republic of Cyprus through the Research Promotion Foundation (Strategic Infrastructure Project NEA ΥΠΟΔΟΜΗ/ΣΤΡΑΤΗ/0308/06). M.V.K. acknowledges financial support from the European Union via FP7 (ERC Starting Grant 2012 "NANOSOLID", contract number 306733).

Received: October 11, 2013
Revised: November 28, 2013
Published online: January 14, 2014

[1] I. Robel, V. Subramanian, M. Kuno, P. V. Kamat, *J. Am. Chem. Soc.* **2006**, *128*, 2385.
[2] G. Konstantatos, I. Howard, A. Fischer, S. Hoogland, J. Clifford, E. Klem, L. Levina, E. H. Sargent, *Nature* **2006**, *442*, 180.
[3] D. V. Talapin, J.-S. Lee, M. V. Kovalenko, E. V. Shevchenko, *Chem. Rev.* **2010**, *110*, 389.
[4] Y. Yin, A. P. Alivisatos, *Nature* **2005**, *437*, 664.
[5] R. Tangirala, J. L. Baker, A. P. Alivisatos, D. J. Milliron, *Angew. Chem. Int. Ed.* **2010**, *49*, 2878.
[6] I. S. Moody, A. R. Stonas, M. C. Lonergan, *J. Phys. Chem. C* **2008**, *112*, 19383.
[7] G. Konstantatos, I. Howard, A. Fischer, S. Hoogland, J. Clifford, E. Klem, L. Levina, E. H. Sargent, *Nature* **2006**, *442*, 180.
[8] D. V. Talapin, C. B. Murray, *Science* **2005**, *310*, 86.
[9] A. G. Dong, X. C. Ye, J. Chen, Y. J. Kang, T. Gordon, J. M. Kikkawa, C. B. Murray, *J. Am. Chem. Soc.* **2011**, *133*, 998.
[10] G. Konstantatos, J. Clifford, L. Levina, E. H. Sargent, *Nat. Photonics* **2007**, *1*, 531.
[11] E. J. D. Klem, H. Shukla, S. Hinds, D. D. MacNeil, L. Levina, E. H. Sargent, *Appl. Phys. Lett.* **2008**, *92*, 212105.
[12] K. Szendrei, M. Speirs, W. Gomulya, D. Jarzab, M. Manca, O. V. Mikhnenko, M. Yarema, B. J. Kooi, W. Heiss, M. A. Loi, *Adv. Funct. Mater.* **2012**, *22*, 1598.
[13] M. V. Kovalenko, M. I. Bodnarchuk, J. Zaumseil, J.-S. Lee, D. V. Talapin, *J. Am. Chem. Soc.* **2010**, *132*, 10085.
[14] A. Nag, M. V. Kovalenko, J.-S. Lee, W. Liu, B. Spokoyny, D. V. Talapin, *J. Am. Chem. Soc.* **2011**, *133*, 10612.
[15] M. V. Kovalenko, R. D. Schaller, D. Jarzab, M. A. Loi, D. V. Talapin, *J. Am. Chem. Soc.* **2012**, *134*, 2457.

[16] J.-H. Choi, A. T. Fafarman, S. J. Oh, D.-K. Ko, D. K. Kim, B. T. Diroll, S. Muramoto, J. G. Gillen, C. B. Murray, C. R. Kagan, *Nano Lett.* **2012**, *12*, 2631.
[17] T. Rauch, M. Boberl, S. F. Tedde, J. Furst, M. V. Kovalenko, G. N. Hesser, U. Lemmer, W. Heiss, O. Hayden, *Nat. Photonics* **2009**, *3*, 332.
[18] S. A. McDonald, G. Konstantatos, S. Zhang, P. W. Cyr, E. J. D. Klem, L. Levina, E. H. Sargent, *Nat. Mater.* **2005**, *4*, 138.
[19] A. G. Pattantyus-Abraham, I. J. Kramer, A. R. Barkhouse, X. Wang, G. Konstantatos, R. Debnath, L. Levina, I. Raabe, M. K. Nazeeruddin, M. Gratzel, E. H. Sargent, *ACS Nano* **2010**, *4*, 3374.
[20] R. Debnath, M. T. Greiner, I. J. Kramer, A. Fischer, J. Tiang, D. A. R. Barkhouse, X. Wang, L. Levina, Z. H. Lu, E. H. Sargent, *Appl. Phys. Lett.* **2010**, *97*, 023109.
[21] G. Konstantatos, E. H. Sargent, *Appl. Phys. Lett.* **2007**, *91*, 173505.
[22] N. Zhao,T. P. Osedach, L. Y. Chang, S. M. Geyer, D. Wanger, M. T. Binda, A. C. Arango, M. G. Bawendi, V. Bulovic, *ACS Nano* **2010**, *4*, 3743.
[23] J. Tang, K. W. Kemp, S. Hoogland, K. S. Jeong, H. Liu, L. Levina, M Furukawa, X. Wang, R. Debnath, D. Cha, K. W. Chou, A. Fischer, A. Amassian, J. B. Asbury, E. H. Sargent, *Nat. Mater.* **2011**, *10*, 765.
[24] M. V. Kovalenko, M. Scheele, D. V. Talapin, *Science* **2009**, *324*, 1417.
[25] W.-K. Koh, S. R. Saudari, A. T. Fafarman, C. R. Kagan, C. B. Murray, *Nano Lett.* **2011**, *11*, 4764.
[26] E. Lhuillier, S. Keuleyan, P. Zolotavin, P. Guyot-Sionnest, *Adv. Mater.* **2013**, *25*, 137.
[27] I. Moreels, K. Lambert, D. Smeets, D. De Muynck, T. Nollet, J. C. Martins, F. Vanhaecke, A. Vantomme, C. Delerue, G. Allan, Z. Hens, *ACS Nano* **2009**, *3*, 3023.
[28] A. Wolcott, V. Doyeux, C. A. Nelson, R. Gearba, K. W. Lei, K. G. Yager, A. D. Dolocan, K. Williams, D. Nguyen, X.-Y. Zhu, *J. Phys. Chem. Lett.* **2011**, *2*, 795.
[29] K. Shimakawa, A. Kolobov, S. R. Elliot, *Adv. Phys.* **1995**, *44*, 475.
[30] D. Tsokkou, G. Itskos, S. Choulis, M. Yarema, W. Heiss, A. Othonos, *Nanotechnology* **2013**, *24*, 235707.
[31] E. Istrate, S. Hoogland, V. Sukhovatkin, L. Levina, S. Myrsko, P. W. E. Smith, E. H. Sargent, *J. Phys. Chem. B* **2008**, *112*, 2757.
[32] M. C. Beard, *J. Phys. Chem. Lett.* **2011**, *2*, 1282.
[33] G. Nootz, L. A. Padilha, L. Levina, V. Sukhovatkin, S. Webster, L. Brzozowski, E. H. Sargent, D. J. Hagan, E. W. V. Stryland, *Phys. Rev. B* **2011**, *83*, 155302.
[34] J. Zhang, X. Jiang, *J. Phys. Chem. B* **2008**, *112*, 32.
[35] P. Andreakou, M. Brossard, C. Li, M. Bernechea, G. Konstantatos, P. G. Lagoudakis, *J. Phys. Chem. C* **2013**, *117*, 1887.
[36] G. Itskos, P. Papagiorgis, D. Tsokkou, A. Othonos, F. Hermerschmidt, S. P. Economopoulos, M. Yarema, W. Heiss, S. Choulis, *Adv. Energy Mater.* **2013,** *3*, 1490.
[37] K. E. Knowles, M. T. Frederick, D. B. Tice, A. J. Morris-Cohen, E. A. Weiss, *J. Phys. Chem. Lett.* **2012**, *3*, 18.
[38] B. Diaconescu, L. A. Padilha, P. Nagpal, Brian, S. Swartzentruber, V. I. Klimov, *Phys. Rev. Lett.* **2013**, *110*, 127406.
[39] F. Gesuele, M. Y. Sfeir, W.-K. Koh, C. B. Murray, T. F. Heinz, C. W. Wong, *Nano Lett.* **2012**, *12*, 2658.
[40] W. W. Yu, L. Qu, W. Guo, X. Pen, *Chem. Mater.* **2003**, *15*, 2854.
[41] O. Madelung, Semiconductor Data Handbook, Springer, Berlin, Germany **2004**.
[42] M. S. Gaponenko, A. A. Lutich, N. A. Tolstik, A. A. Onushchenko, A. M. Malyarevich, E. P. Petrov, K. V. Yumashev, *Phys. Rev. B* **2010**, *82*, 125320.
[43] G. Itskos, A. Othonos, T. Rauch, S. F. Tedde, O. Hayden, M. V. Kovalenko, W. Heiss, S. A. Choulis, *Adv. Energy Mater.* **2011**, *1*, 802.
[44] S. R. Johnson, D. Ding, J.-B. Wang, S.-Q. Yu, Y.-H. Zhang, *J. Vac. Sci. Technol. B* **2007**, *25*, 1077.
[45] L. A. Padilha, I. Robel, D. C. Lee, P. Nagpal, J. M. Pietryga, V. I. Klimov, *ACS Nano* **2011**, *5*, 5045.
[46] A. M. Andriesh, D. I. Tsiulyanu, *J. Non-Cryst. Solids* **1987**, *97-98*, 1135.
[47] M. A. Hines, G. D. Scholes, *J. Am. Chem. Soc.* **2011**, *133*, 10612.